ELSEVIER

Physica A 263 (1999) 284–292

PHYSICA A

Relaxation of 2D Turbulence to Vortex Crystals

C.F. Driscoll, D.A. Schecter, D.Z. Jin, D.H.E. Dubin, K.S. Fine, and A.C. Cass

Physics Department, Univ. of California, San Diego, La Jolla, California 92093, USA

Abstract

A magnetically confined electron column evolves in (r, θ) as an essentially inviscid, incompressible 2D fluid with a single sign of vorticity. Turbulent initial states with 50–100 vortices relax due to vortex merger and filamentation, in general agreement with recent scaling theories. However, this relaxation is sometimes halted when 3–20 vortices "anneal" into a fixed pattern, or "vortex crystal." 2D vortex-in-cell simulations reproduce this effect, demonstrating that the vortex "cooling" is independent of fine-scale viscosity, but strongly dependent on the strength of the weak background vorticity. A new "restricted maximum fluid entropy" theory predicts the crystal patterns and background vorticity distribution, by assuming conservation of the robust flow invariants and preservation of the intense vortices.

1 Introduction

Magnetically confined pure electron columns are excellent systems for quantitative observations of 2D vortices, turbulence and self-organization [1]. A "generic" experimental apparatus is shown schematically in Fig. 1. The electrons are contained in a grounded conducting cylinder. A uniform axial magnetic field ($B \lesssim 1$T) provides radial confinement, and negative voltages ($V \lesssim 600$. Volts) applied to end cylinders provide confinement at the ends.

The apparatus is operated in an inject/manipulate/dump-and-measure cycle. For injection the leftmost cylinder is briefly grounded, allowing electrons to enter from the negatively biased tungsten filament. Then the confined plasma is sensed and manipulated by antennas on the wall. Finally, after a confinement time which may be as long as hundreds of seconds, the rightmost cylinder is grounded and the z-integrated electron density $n(r, \theta, t)$ is measured by accelerating the electrons onto a phosphor screen and imaging the resulting light with a CCD camera.

For the experiments discussed here, the electron gyrofrequency is a few GHz, which is much higher than other frequencies in the system. The gyroradius is the order of a few μm, which is much smaller than the diameter of the conducting wall ($2R_w = 7$ cm). In addition, the density is far below the Brillouin limit ($n/n_B \sim .01$), *i.e.* electrons move slowly enough so that electron inertia can be ignored. In this regime the electron velocity is well-described by $\mathbf{E} \times \mathbf{B}$ drifts as $\mathbf{v}(r, \theta, t) = \mathbf{E} \times \mathbf{B}/B^2$. Finally, the individual electrons

0378-4371/99/$ – see front matter
PII: S0378-4371(98)00495-6

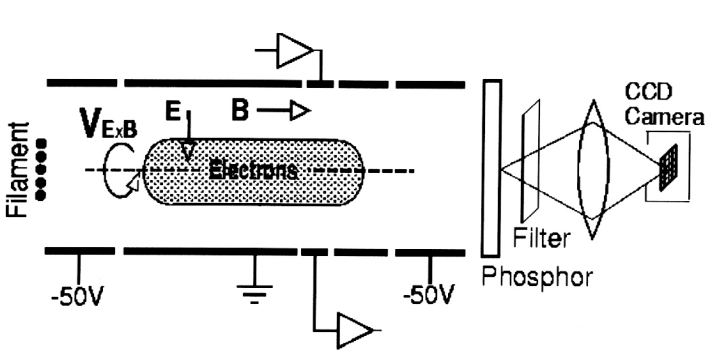

Fig. 1. The cylindrical experimental apparatus with phosphor screen/CCD camera diagnostic.

move rapidly along the magnetic field lines, bouncing between the ends of the plasma at a frequency of order 1 MHz. This axial bounce frequency is much larger than the drift rotation frequency (10–100 kHz) of the column, so the electrons behave as rigid "bounce-averaged rods" of charge.

In this approximation, the (r,θ) flow of the electrons is described by the 2D drift-Poisson equations [1], which can be written in terms of the vorticity $\zeta(r,\theta,t) \equiv (4\pi ec/B)n$ and the scaled potential $\psi(r,\theta,t) \equiv (c/B)\phi(r,\theta,t)$ as

$$\frac{\partial \zeta}{\partial t} + \mathbf{v}\cdot\nabla\zeta = 0\,, \quad \mathbf{v} = -\nabla\psi \times \hat{z}\,,$$

$$\nabla^2\psi = \zeta\,.$$

The drift-Poisson equations are thus isomorphic to the Euler Equations. We emphasize that the flow vorticity is proportional to the electron density, which is directly measured. A column of electrons in vacuum surrounded by a conductor thus evolves as would a 2D vortex in an incompressible inviscid fluid surrounded by a circular free-slip boundary. Of course, there are also unwanted diffusive effects due to the end confinement fields and "viscous" effects on small spatial scales due to electron-electron collisions, which are *not* modeled by the Euler *or* the Navier-Stokes equation. However, we believe the effects described in this paper do not depend on the details of the fine-scale dissipation.

Euler flows are strongly constrained by integral invariants. The total circulation (number of electrons), scaled angular momentum, and scaled electrostatic energy, given by

$$\Gamma_{\rm tot} \equiv \int d^2\mathbf{r}\,\zeta\,,$$

$$P_\theta \equiv R_w^{-2}\int d^2\mathbf{r}\,(1-r^2)\,\zeta/\zeta_0\,,$$

$$H \equiv -(1/2)\,R_w^{-2}\int d^2\mathbf{r}\,(\zeta/\zeta_0)\,(\psi/\psi_0)\,,$$

are well conserved. Here, $\zeta_0 \equiv \Gamma_{\rm tot}/R_w^2$ and $\psi_0 = \Gamma_{\rm tot}/4\pi$. However, less robust invariants such as enstrophy and mean-field entropy, given by

$$Z_2 \equiv (1/2)\,R_w^{-2}\int d^2\mathbf{r}\,(\zeta/\zeta_0)^2\,,$$

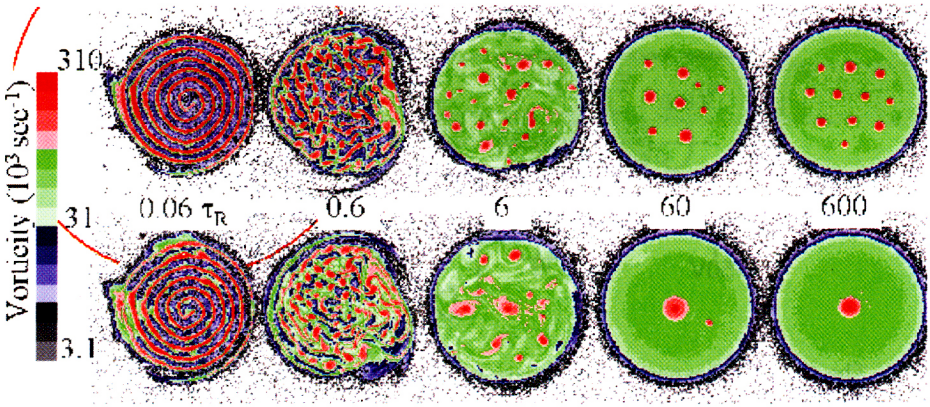

Fig. 2. Images of vorticity at five times for two sequences from similar initial conditions.

$$S \equiv -R_w^{-2} \int d^2\mathbf{r}\ (\zeta/\zeta_0)\ \ln(\zeta/\zeta_0)\ ,$$

vary significantly, due to measurement coarse-graining or dissipation of small spatial scales.

2 Relaxation to Vortex Crystals

We start with highly filamented initial conditions, which rapidly form 50-100 vortices, and then freely relax toward a 2D meta-equilibrium. Here, chaotic mutual advection and vortex merger are clearly important dynamical processes, and the final meta-equilibrium is typically strongly peaked on center. Surprisingly, this relaxation is sometimes halted when individual vortices settle into a stable, rotating crystalline pattern which lasts for thousands of rotation times.

Figure 2 shows the measured z-averaged electron density $n(r,\theta,t)$ at five times for two slightly different initial conditions: the upper sequence forms vortex crystals, whereas the lower sequence relaxes rapidly to a monotonically-decreasing profile [2]. The observed vortex crystal states consists of 5-20 individual vortices each 4-6 times the background vorticity, arranged in a lattice pattern which rotates with the background. That is, rods of enhanced electron density ($n \sim 7 \times 10^6$ cm^{-3}) are maintaining self-coherence and positions relative to each other for several seconds, while $\mathbf{E} \times \mathbf{B}$ drifting with a diffuse background ($n_B \sim 2 \times 10^6$ cm^{-3}). Vortex crystal states are repeatably observed over a range of filament bias voltages, but the characteristics of $n(r,\theta)$ required for these states are not yet understood.

Figure 3 shows the number of distinct vortices N_v, and the enstrophy Z_2 for the two sequences. In each sequence, the unstable filamentary initial condition forms $N_v = 50-100$ vortices of roughly equal circulation, after which N_v initially decreases as $N_v \sim t^{-\xi}$, with $\xi \approx 1$. This relaxation is generally consistent with a dynamical scaling based on conserved quantities in repeated vortex merger [3]. The observed ξ range from 0.2 to 1.1 as the initial

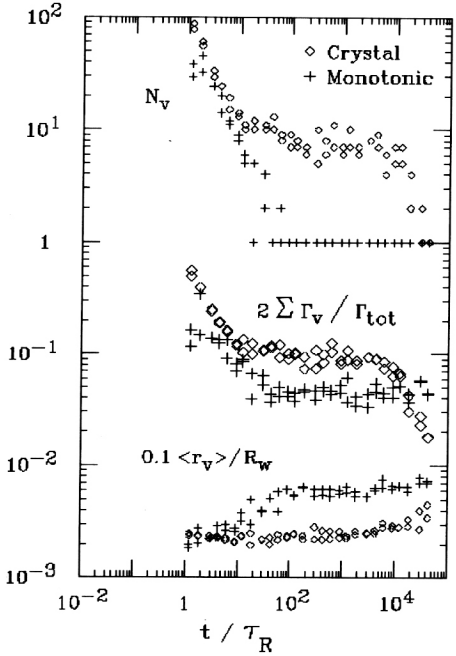

Fig. 3. Number of surviving vortices N_v, their circulation $\sum \Gamma_v$, and their average radius $< r_v >$ for the two evolutions of Fig. 2.

conditions are varied, with 0.8 being commonly observed.

In the evolution of the top sequence in Fig. 2, the relaxation is arrested by the "cooling" of the chaotic vortex motions, with formation of vortex crystals by $10\tau_R$. (Here, $\tau_R = 170\mu$s.) The diamonds in Fig. 3 show that 8 to 10 distinct vortices survive for about $10^4\tau_R$. Since the vortices all have about the same circulation, the patterns are quite regular, as seen at $600\tau_R$ in Fig. 2. After $10^4\tau_R$, N_v decreases to 1 as the individual vortices decay away in place due to non-ideal "viscous" effects. Other experimental images show that as N_v decreases, the remaining vortices re-adjust to a new rigidly rotating, symmetrically spaced pattern.

The measured integral quantities for both sequences are consistent with 2D inviscid motion on large scales and dissipation on fine scales. Experimentally, the circulation, angular momentum, and energy are robust invariants. In contrast, the enstrophy Z_2 is a "fragile" invariant, and initially decays a factor of about 4 in both sequences. For the crystal sequence, Z_2 is constant from $10\tau_R$ until $10^4\tau_R$, after which time the individual vortices decay in place due to non-ideal effects.

Reduction of the chaotic advective motions of the individual vortices is required to form the vortex crystal states. Figure 4 shows that the average magnitude of the random velocities of the individual vortices, $|\delta V|$, decreases by a factor of 6 between 2 τ_R and 100 τ_R for the crystals sequence, whereas only slight cooling is seen before $N_v = 1$ for the

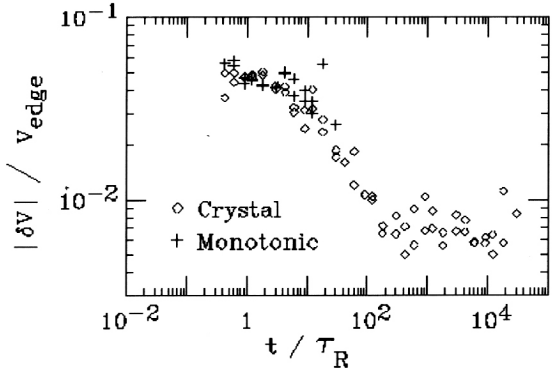

Fig. 4. Decrease in the average random vortex velocity $|\delta V|$ as the crystal sequence "cools."

monotonic sequence [2].

We believe this cooling and cessation of relaxation through mergers is a near-inviscid 2D fluid effect, *i.e.* independent of the details of the fine-scale dissipation. However, two essential characteristics of this system are the non-zero total circulation and the boundary of the vorticity patch; these effects may not be present in other systems. Here, because there is no "negative" vorticity, the diffuse background necessarily persists, and the vortex/background interactions are more pronounced.

3 2D Vortex-In-Cell Simulations

In order to show that the cooling of turbulent flow to vortex crystals is a 2D inviscid effect, we compare the experiments directly to vortex-in-cell simulations [4] that approximate 2D Euler dynamics. We will see that the experiments and simulations cool at the same rates to vortex crystals with similar vorticity distributions. Varying the discreteness of the simulation presumably varies the non-ideal viscous effects, but this does not affect the cooling. Further, the simulations can artificially vary the strength of the background vorticity, and this is seen to strongly affect the cooling.

In the simulation, 8×10^5 microscopic point vortices are distributed to match the measured initial vorticity profile of the experiment. The vorticity is interpolated from the particles to a 513×513 square grid on which Poisson's equation is solved with the boundary condition $\psi(R_w, \theta) = 0$. Poisson's equation is solved with a five-point finite difference scheme that employs multigrid relaxation. The velocity field is obtained on the grid by taking the gradient of ψ and is then interpolated to the point-vortex positions. The point-vortices move forward in time with second-order Adams-Bashforth steps. By construction, the simulations conserve Γ_{tot}. They also conserve H and P_θ to about one part in 10^3.

Several simulations have been done, starting from initial conditions which are an experimental image of $\zeta(r, \theta)$ at a chosen time. Here, we will discuss a simulation begun from an experimental image at $t = 4\tau_R$ in the sequence of Fig. 2. There are subtle differences

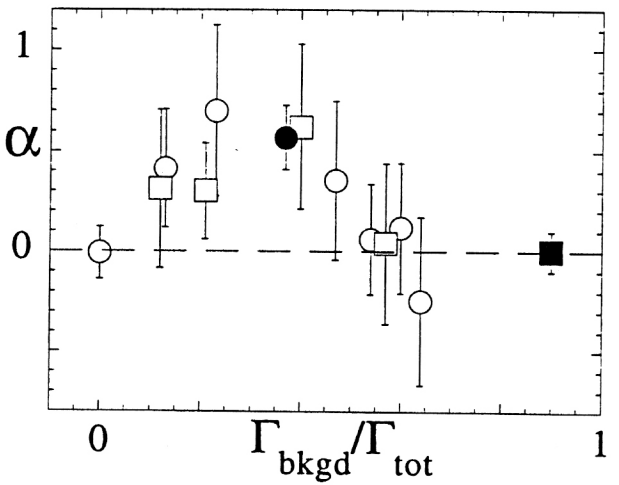

Fig. 5. Cooling exponent α versus relative strength of the background vorticity.

between the simulation and experiment, but they show good quantitative agreement in the number of discrete vortices, $N_v(t)$, and in the rate of cooling of the chaotic vortex motions as measured by $|\delta V|$.

The cooling curves are approximately the same in simulation and experiment, and they appear to follow power law decay as $|\delta V| \propto t^{-\alpha}$. Linear least-squares fits to log-log plots of the data give $\alpha_{\text{sim}} = 0.5 \pm 0.2$ and $\alpha_{\text{exp}} = 0.4 \pm 0.1$ during the initial phase of the flow.

Simulations with a different number of point vortices have verified that the vortex cooling and crystallization is not sensitive to this discreteness. The point vortex gas is equivalent to an ideal Euler fluid only in the mean field approximation. Microscopic fluctuations of the vorticity about the mean field cause distributions of point-vortices to eventually relax to global maximum entropy states.

We examined the importance of this microscopic collisionality on cooling and vortex crystal formation by changing the number of point-vortices in a simulation from 8×10^5 to 4×10^5 to 1×10^5. For all three cases, the total circulation of the discrete vortices, $\sum \Gamma_{\text{d.v.}}$, remained the same within 5%, and the cooling curves are roughly equivalent. This result indicates that non-ideal effects from the finite number of point vortices in the simulation is not important to the observed vortex cooling; and it also suggests that these effects are not dominant in the experiments.

We believe that cooling occurs through the turbulent mixing of background vorticity by the strong discrete vortices. To test this, we start with the simulated flow at $t = 14\tau_R$, then we artificially multiply all "background" vorticity by a constant ranging from 0 to 3. Evolving this artificial system forward, we observe cooling which depends on the strength of the background vorticity. Figure 5 shows the cooling exponent α versus $\Gamma_{\text{bkgd}}/\Gamma_{\text{tot}}$. Squares correspond to the flow in Fig. 2 and circles correspond to a (substantially different) annular initial condition which also relaxes to vortex crystals. There is no cooling in the absence of the background, and there is no cooling if almost all of the circulation is in the background. When the background is too strong, cooling is apparently countered by

shears and fluctuations in the background vorticity.

4 Regional Maximum Fluid Entropy Theory

In recent years, two radically different theories have had success in describing the free relaxation of 2D turbulence. One is the global maximum fluid entropy (GMFE) theory [5], which approximates the turbulent flow as a collection of non-overlapping, incompressible microscopic vorticity elements that become ergodically mixed in the relaxed state. The other theory is the punctuated scaling theory (PST) [3], which states that the turbulent flow is dominated by well-separated strong vortices which follow Hamiltonian dynamics of point vortices, punctuated by the occasional merger of like-sign vortices. The relaxed state is then one vortex of each sign, or just one vortex in our case.

However, neither of these theories provides a complete description for all 2D turbulent flows. Clearly, the GMFE theory cannot explain the vortex crystals, since the theory predicts a smooth vorticity distribution. The PST predicts the observed power law decrease in the number of strong vortices, but the theory does not explain why several strong vortices remain and anneal into an equilibrium pattern in the final state of the turbulent relaxation.

A new theory approach [6] characterizes the vortex crystal states by maximizing the fluid entropy in the presence of persistent strong vortices. The key idea is that some regions of the flow are well-mixed, while other regions are not. The strong vortices ergodically mix the background, driving it into a state of maximum fluid entropy. This mixing, in return, affects the punctuated dynamics of the strong vortices, "cooling" their chaotic motion, and driving them into an equilibrium pattern. However, the vorticity in the strong vortices is trapped and remains unmixed. The resulting equilibrium is called a "regional" maximum fluid entropy (RMFE) state, in order to distinguish it from the GMFE state that allows no unmixed regions and hence no surviving strong vortices.

The quantities that determine the RMFE state include the conserved quantities of the measured flow that survive coarse graining: the total circulation $\Gamma_{\rm tot}$, the angular momentum P_θ, and the energy H. The diffuse background vorticity is assumed to consist of incompressible microscopic vorticity elements of fixed strength ζ_f, with ζ_f taken to be the maximum observed vorticity. Coarse-graining over these randomized vorticity elements gives the observed background vorticity $\zeta_b(r)$.

In addition to the above quantities, we need to know the number M of surviving strong vortices and their vorticity distributions $\{\zeta_i(r),\ i = 1,2...M\}$. These properties of the strong vortices depend on the details of the early evolution of the flow, and are beyond the scope of the statistical theory. The statistical theory treats the flow only after the mergers of the strong vortices have ceased.

Given these inputs, two properties of the relaxed vortex crystal state can be predicted: the coarse-grained vorticity distribution of the background $\zeta_b(r)$, and the equilibrium positions $\{\mathbf{R}_i\}$ of the strong vortices. The equations that characterize the RMFE states are obtained by maximizing the fluid entropy $S[\zeta_b(\mathbf{r})]$ associated with the background distribution $\zeta_b(\mathbf{r})$. This entropy can be calculated by counting the number of ways of arranging microscopic vorticity elements, each with vorticity ζ_f, to obtain the given coarse-grained vorticity $\zeta_b(r)$.

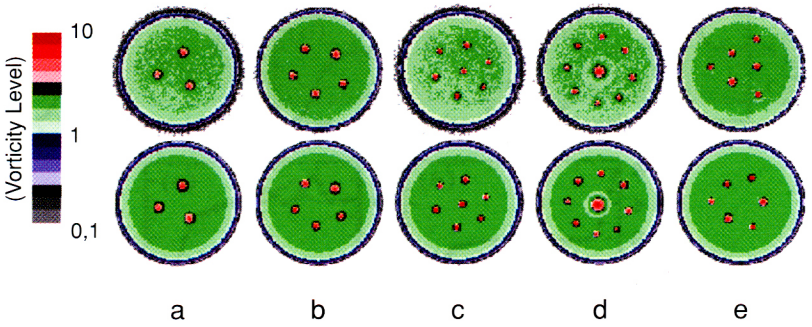

Fig. 6. A selection of experimentally observed vortex crystal patterns (top), and the patterns predicted by RMFE theory (bottom).

The maximization of S while keeping H, L and Γ constant is done by finding the extrema of $S' \equiv S - \beta(H - \Omega P_\theta + \mu\Gamma)$ with respect to the independent variables $\{\mathbf{R}_i\}$ and $\zeta_b(\mathbf{r})$. Here β, Ω and μ are Lagrange multipliers that can be interpreted as inverse "temperature", rotation frequency and chemical potential. Maximization with respect to ζ_b gives

$$\zeta_b(\mathbf{r}) = \zeta_f / (e^{\beta\zeta_f \Psi} + 1),$$

where $\Psi \equiv \psi + \frac{1}{2}\Omega r^2 + \mu$ is the stream function in the rotating frame. This is analogous to the Fermi distribution in quantum statistics, which is to be expected, since the microscopic vorticity elements are incompressible. Maximization with respect to $\{\mathbf{R}_i\}$ yields $\partial[H - \Omega P_\theta] / \partial\mathbf{R}_i = 0$. This equation states that the strong vortices are stationary in a frame rotating with frequency Ω, implying that they form a vortex crystal equilibrium. The parameters β, Ω, μ, $\{R_i\}$ are then varied numerically until the solution has the proper Γ_{tot}, P_θ and H_ϕ.

The RMFE solutions reproduce the observed vortex crystal patterns, as shown in Fig. 6. Also, the observed background vorticity is close to the theory, as can be seen in the θ−averaged vorticity profiles shown in Fig. 7. The edge of the background distribution falls off gradually, since the vorticity elements near the edge can fluctuate in energy by an amount of order $1/\beta$. Also, near a strong vortex the background vorticity is slightly depressed, since ψ tends to increase due to the influence of the strong vortex, as can be observed around the large central vortex in Fig. 6(d).

Some of the patterns agree more closely with the theory than others; there are deviations both in the geometry of the intense vortices, and in the shape of the background vorticity edge. Analysis of ≈ 25 experimental images shows that both of these deviations decrease markedly with time during the evolution. Image 6(e) was taken at about $300\tau_R$, whereas the other images were taken at $(2000-20,000)\tau_R$. The final cooling process can apparently be quite weak.

Thus, the following physical picture of vortex crystal formation emerges: the strong vortices undergo chaotic mergers described by punctuated scaling theory, but they also ergodically mix the low vorticity background. The mixing of the background, in return,

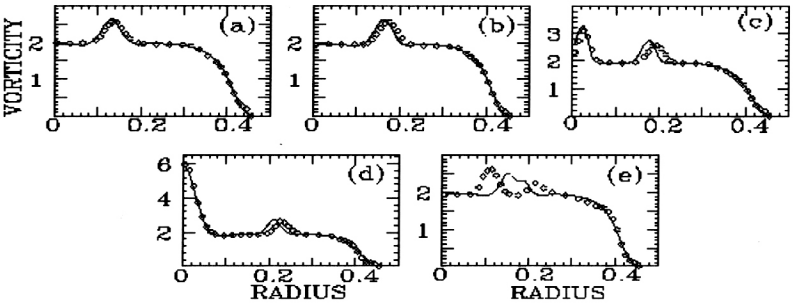

Fig. 7. Measured and predicted theta-averaged vorticity distributions for the 5 vortex crystals of Fig. 6.

cools the chaotic motions of the strong vortices, and drives the strong vortices into a vortex crystal equilibrium. This picture shows that the interaction between the strong vortices and the background, a process neglected in the PST, can be important in understanding the relaxation of 2D turbulence. It also shows that fluid entropy maximization can provide useful results for the relaxed state, provided one recognizes that in general only certain parts of the flow may be well-mixed.

5 Acknowledgments

This work was supported by National Science Foundation grant PHY94-21318 and Office of Naval Research Grant N00014-96-1-0239.

References

[1] C.F. Driscoll and K.S. Fine, "Experiments on Vortex Dynamics in Pure Electron Plasmas," Phys. Fluids **2**, 1359 (1990).

[2] K.S. Fine, A.C. Cass, W.G. Flynn and C.F. Driscoll, "Relaxation of 2D Turbulence to Vortex Crystals," Phys. Rev. Lett. **75**, 3277 (1995).

[3] G.F. Carnevale *et al.*, Phys. Rev. Lett. **66**, 2735 (1991); J.B. Weiss and J.C. McWilliams, Phys. Fluids A **5**, 608 (1993).

[4] D.A. Schecter, D.H.E. Dubin, K.S. Fine, and C.F. Driscoll, "Vortex Crystals from 2D Euler Flow: Experiment and Simulation," submitted to Phys. Fluids.

[5] J. Miller, Phys. Rev. Lett. **65**, 2137 (1990); R. Robert and J. Sommeria, J. Fluid Mech, **229**, 291 (1991); J. Miller, P.B. Weichman, and M.C. Cross, Phys. Rev. A **45**, 2328 (1992), and references therein.

[6] D.Z. Jin and D.H.E. Dubin, "Regional Maximum Entropy Theory of Vortex Crystal Formation," Phys. Rev. Lett. **80**, 4434-4437 (1998).